Efficiency of TV-regularized algorithms in computed tomography with Poisson-Gaussian noise

Théo Leuliet[1], Louise Friot--Giroux[1], Walid Baaziz[2],
Élie Bretin[3], Ovidiu Ersen[2], Françoise Peyrin[1], Bruno Sixou[1], Voichiţa Maxim[1]
[1] *CREATIS, INSA-Lyon, Université de Lyon, FRANCE*
{*theo.leuliet, louise.friot--giroux, francoise.peyrin, bruno.sixou, voichita.maxim*}*@creatis.insa-lyon.fr*
[2] *Institut de Physique et Chimie des Matériaux de Strasbourg, Université de Strasbourg, FRANCE, ovidiu.ersen@ipcms.unistra.fr*
[3] *Institut Camille Jordan, INSA-Lyon, Université de Lyon, FRANCE, elie.bretin@insa-lyon.fr*

***Abstract*—Regularized algorithms are the state-of-the-art in computed tomography, but they are also very demanding in computer resources. In this work we test two data-fidelity formulations and some associated algorithms for the resolution of the Total-Variation regularized tomographic problem. We compare their computational cost for a mixture of Poisson and Gaussian noises. We show that a recently proposed MAP-EM algorithm outperforms the TV-regularized SIRT and the Chambolle-Pock algorithms on synthetic data for the considered noise. We illustrate this result on experimental data from transmission electron microscopy.**

***Index Terms*—Tomographic reconstruction, Poisson noise, Gaussian noise, electron microscopy, total variation, FISTA**

I. Introduction

Tomographic reconstruction aims at finding an object f from its projections p. Knowing the forward projection operator A, the associated linear inverse problem consists in finding f from:

$$Af = p. \tag{1}$$

In every realistic application of this reconstruction process, the data are corrupted by some noise and neither the existence nor the uniqueness of the solution are guaranteed; moreover the solution does not necessarily depend continuously on the data. As a consequence, even if analytic algorithms like Filtered Back Projection (FBP) are fast, they cannot take into account a lot of elements such as physical constraints of the detector, statistic fluctuations, attenuation or diffusion. The noise corrupting the projection reduces the performance of these algorithms. Variational approaches are often used to reconstruct the object f. Instead of directly computing an analytic solution to the problem (1), a functional is minimized over the set of potential solutions f. It consists of a data consistency term $d(Af, p)$ and a penalty term $R(f)$, leading to the general optimization problem:

$$f^* = \underset{f}{\operatorname{argmin}}\, d(Af, p) + R(f). \tag{2}$$

The authors acknowledge financial support of the French National Research Agency through the ANR project 3DCLEAN (ANR-15-CE09-0009) and LABEX PRIMES (ANR-11-IDEX-0007) of Université de Lyon.

The data consistency reflects knowledge on statistical properties of the noise and the penalty forces the solution to satisfy some prior information on the unknown object. Equation (2) is solved using iterative methods. In transmission tomography, where the noise is generally considered as Gaussian, the most common algorithms are ART (Algebraic Reconstruction Technique [1]), SART (Simultaneous Algebraic Reconstruction Technique [2]) and SIRT (Simultaneous Iterative Reconstruction Technique [3]). In emission tomography and for Poisson noise, MLEM (Maximum Likelihood Expectation Maximization [4]) and its variants are more widespread. These algorithms ignore prior information on the data. However, they can be enhanced to allow penalized problems solving by considering them as EM (Expectation-Maximization) algorithms [5]. Instances of such MAP (Maximum-A-Posteriori) EM algorithms are [6] for SIRT algorithm and [7] for the MLEM algorithm with TV (Total Variation) regularization. More recently, a convergent algorithm was developed specifically for Poisson noise in [8]. Problem (2) can also be solved by general convex optimization algorithms. Very few studies deal with the mixed Poisson-Gaussian noise often encountered in real data [9], [10]. In this case, the noise statistics leads to an infinite sum in the log-likelihood function which is difficult to evaluate numerically. The Poisson-Gaussian model is often simplified with variance stabilization techniques [11]. In this work, we consider a mixed Poisson-Gaussian noise and we compare three existing algorithms with either the ℓ_2 norm or Kullback-Leibler distance as discrepancy term and with the total variation as regularization term: Chambolle-Pock algorithm [12], SIRT-FISTA-TV [6] and a FISTA accelerated version of the algorithm from [8] that we call EM-FISTA-TV. We compare them in terms of quality of reconstruction and computational efficiency on simulated and experimental data from transmission electron microscopy.

II. Reconstruction methods

A. Data fidelity terms and minimization algorithms

In (2), the first term of the functional represents the gap between data and the projection of the solution. The choice of this distance reflects the statistics of the noise. We consider

here both the quadratic $d_q(Af,p) = \|Af - p\|_2^2$ and the Kullback-Leibler distance defined as:

$$d_{KL}(Af,p) = \sum_i [Af - p\log(Af)]_i \tag{3}$$

The product as well as the division of vectors are considered element-wise. These distances are the loss functions associated to pure Gaussian or Poisson noises.

1) SIRT: The first iterative algorithm for image reconstruction, called ART [1], consisted in solving (1) by iteratively projecting the current solution on hyperplanes formed by the underlying system of equation. SIRT [2] turned out to be more stable in the case of noisy projections. We denote I as the image space, P as the projection space and $\mathbf{1}$ a vector of ones with appropriate dimension. The general formulation of the algorithm is then:

$$f^{(n+1)} = f^{(n)} + \lambda \frac{1}{A^*\mathbf{1}_P} A^* \left[\frac{p - Af^{(n)}}{A\mathbf{1}_I}\right] \tag{4}$$

with A^* the adjoint of the projection matrix A and λ the update parameter. At each iteration the weighted differences between the projections of the current image and the actual projections are back-projected then subtracted from the current image. SIRT can be interpreted as a weighted gradient descent for minimizing the distance $||Af - p||_2^2$.

2) MLEM: When the data is Poisson distributed, the EM methodology leads to the algorithm:

$$f^{(n+1)} = \frac{f^{(n)}}{A^*\mathbf{1}_P} A^* \left[\frac{p}{Af^{(n)}}\right] \tag{5}$$

High frequencies are introduced faster than in SIRT, and the result tends to become very noisy. In practice a convenient solution is obtained by early stopping and smoothing. MLEM is also a weighted gradient-descent algorithm for the minimization of the d_{KL} distance.

B. TV regularization

Initially proposed for image denoising [13], TV regularization has proven to be really efficient in inverse problems to restore piecewise constant images, as in [14]. For smooth images, the TV-norm of an image f can be defined as $TV(f) = \||\nabla f|\|_1$, where ∇ is the gradient operator and $\||\cdot|\|_1$ is the ℓ_1 norm of the gradient, *i.e.,* the sum of modulus of gradients for all pixels in the image. The success of TV regularization relies on allowing solutions to preserve edges whilst smoothing flatter regions and gives effective results in missing angle tomography (see *e.g.,* [6]) and in low-statistics emission tomography acquisitions ([7]). The TV term is non-differentiable and variational approaches are often based on the convex duality theory. We introduce below three algorithms used in TV regularization.

1) Chambolle-Pock primal-dual algorithm for Poisson data: Introduced in [12] for a large class of optimization problems, this algorithm can be used to solve for the minimum of:

$$d_{KL}(Af,p) + \delta_P(Af) + \beta TV(f), \tag{6}$$

where P is the projections space corresponding to the range of A. This problem is then solved with a primal-dual approach, performing at each iteration one step for decreasing the data consistency term and one denoising step. We employ here its preconditioned version from [15].

2) MAP-EM algorithms: Adding TV regularization within a EM approach leads to algorithms composed of two nested loops. The outer loop performs image reconstruction and aims to increase the likelihood of the data. It is the same as SIRT for Gaussian distributions and MLEM for Poisson distributions. The inner loop is a denoising algorithm for the same data distribution, applied to the current solution $f^{(n+1/2)}$.

For Gaussian data, the denoising problem:

$$\min_u \frac{\|u - f^{(n+1/2)}\|_2^2}{2} + \beta TV(u), \tag{7}$$

can be solved for instance with the Chambolle's [16] algorithm:

$$u^* = f^{(n+1/2)} - \beta \operatorname{div} \phi^*, \tag{8}$$

with the divergence $\operatorname{div}\phi^* = \nabla \cdot \phi^*$ and ϕ^* the limit of

$$\phi^{(k+1)} = \frac{\phi^{(k)} + \tau\nabla(\operatorname{div}\phi^{(k)} - f^{(n+1/2)}/\beta)}{1 + \tau|\nabla(\operatorname{div}\phi^{(k)} - f^{(n+1/2)}/\beta)|} \tag{9}$$

and τ is an update parameter that satisfies $0 < \tau \leq 1/8$ for two-dimensional images.

This method was adapted in [7] to Poisson distributed data, using an approximation that allows to replace the Kullback-Leibler distance with a weighted quadratic distance. The exact MAP-EM formulation leads to the denoising problem:

$$\operatorname*{argmin}_u \langle u - f^{(n+1/2)}\log u, s\rangle + \beta TV(u), \tag{10}$$

where we note $s = A^*\mathbf{1}_P$ the sensitivity vector. When s is a constant vector, (10) becomes regular Poisson denoising. This functional could be minimized with the Chambolle-Pock algorithm. When the level of noise is small, as it could be the case when the algorithm is applied at each iteration of MLEM, solving the dual problem might be faster [8]. The solution writes:

$$f^{(n+1)} = \frac{sf^{\left(n+\frac{1}{2}\right)}}{s + \beta \operatorname{div}\phi^*}, \tag{11}$$

where the dual solution ϕ^* is obtained iteratively as limit of:

$$\phi^{(k+1)} = \frac{\phi^{(k)} - \tau z^{(k)}}{1 + \tau|z^{(k)}|} \tag{12}$$

with $z^{(k)} = \nabla\left(\frac{sf^{(n+1/2)}}{s + \operatorname{div}\phi^{(k)}}\right)$. The convergence of the algorithm is guaranteed as soon as $\beta \leq \min(s)/4$ and $0 < \tau \leq \frac{(\min(s) - 4\beta)^2}{8\beta\|sf^{(n+1/2)}\|_\infty}$ for two-dimensional images.

C. FISTA acceleration

FISTA ([17]) is an acceleration technique that increases the convergence rate of first order (or gradient) methods for non-smooth convex problems. As both SIRT and MLEM can be seen as gradient descent methods, FISTA acceleration can be used. A sequence of scalars is computed as $t^{(0)} = 1$ and

$$t^{(n+1)} = \frac{1 + \sqrt{1 + 4(t^{(n)})^2}}{2} \tag{13}$$

then the image at iteration $n + 1$ is calculated from the smoothed solutions as:

$$\widetilde{f}^{(n+1)} = f^{(n+1)} + \left(\frac{t^{(n)} - 1}{t^{(n+1)}}\right)\left(f^{(n+1)} - f^{(n)}\right) \tag{14}$$

It is proved in [17] that FISTA can attain a convergence rate of $O(1/n^2)$. A FISTA accelerated version of SIRT-TV, called SIRT-FISTA-TV, was proposed in [6]. The accelerated version for Poisson data was tested in [8]. We call it hereafter EM-FISTA-TV and we additionally apply FISTA acceleration to the denoising step rewritten as a projected gradient.

III. Numerical experiments

In this section, we compare the different reconstruction methods. We show some quantitative results on synthetic data for a fixed setting of noise and an example of three-dimensional reconstruction for a transmission electron microscopy sample.

A. Simulations details

We used a 256×256 pixels Shepp-Logan phantom represented in Fig. 1. Projections and back-projections were computed on GPU thanks to ASTRA Toolbox [18] in Python. The TV denoising was also implemented on GPU to fasten computation. We performed tests where the contribution of Poisson and Gaussian noises are almost equal. In the results we show, the dataset is constructed as follows : random values are drawn from a Poisson law with mean the exact projections, followed by the addition of a zero-mean Gaussian noise with standard deviation $\sigma = 2\%$ of the maximum value in the projections. In this setting the ratio of the standard deviations for both simulated noises equals 1. Note that the standard deviation for Poisson noise is estimated as the mean value of the square root of the projections. Other tests have been performed with different noise configurations - by varying both σ and the pixel intensities in the initial image - with a ratio close to 1, and conclusions are very similar to what we present here. The number of iterations to convergence within the internal denoising loop was fixed to 100 for SIRT-FISTA-TV and 30 for EM-FISTA-TV. The reconstruction quality was measured with the Mean Squared Error (MSE). The convergence speed of the different algorithms was calculated in terms of outer (*i.e.,* reconstruction) iterations and time; for this we have studied the decrease of both the MSE and the cost function. The regularization parameter has a major influence on the reconstructed solutions. In our work we restricted to a basic approach where we study a range of different parameters to find the best reconstruction results.

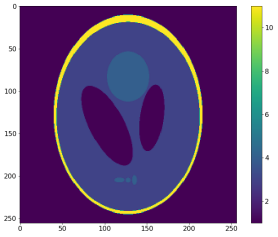

Fig. 1: Shepp Logan phantom used for experiments

B. Computational efficiency for simulated data

Reconstructed images of the Shepp-Logan phantom are represented in Fig. 2 for the Filtered Back-Projection (FBP) algorithm with Hamming filtering and for the three algorithms we discussed earlier.

At convergence, the values of the MSE are respectively 0.13 for EM-FISTA-TV and PCP and 0.16 for SIRT-FISTA-TV. In our tests, these two algorithms outperform SIRT-FISTA-TV for configurations with equal mean standard-deviation contributions from Poisson and Gaussian noises.

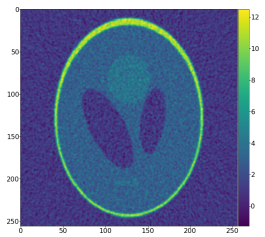

(a) Filtered Back-Projection

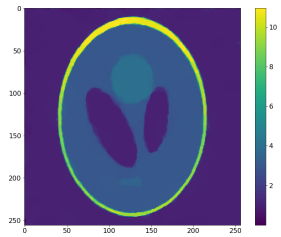

(b) SIRT-FISTA-TV - MSE = 0.16

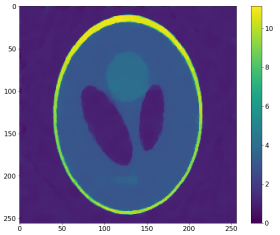

(c) EM-FISTA-TV - MSE = 0.13

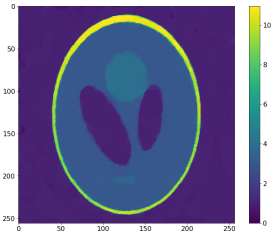

(d) PCP - MSE = 0.13

Fig. 2: Reconstructed images of the Shepp-Logan phantom.

Each iteration of SIRT-FISTA-TV and EM-FISTA-TV requires the computation of a projection and a back-projection in the outer loop, followed by the resolution of a denoising problem. PCP is made of a single loop, making each iteration shorter. When the number of outer iterations is considered, the EM-FISTA-TV algorithm outperforms the two others presented in section II-B (Fig. 3).

We calculated the cost function $d_{KL}\left(Af^{(n)}, p\right) + \beta TV\left(f^{(n)}\right)$ for PCP and EM-FISTA-TV, both derived for Poisson distributions, as a function of the iteration number n. The results are shown in Fig. 4. SIRT-FISTA-TV was not included in the comparison as this algorithm is tailored for Gaussian noise.

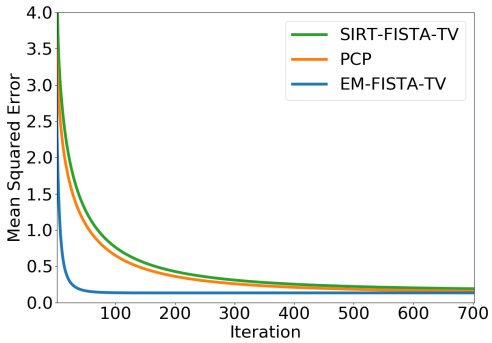

Fig. 3: Evolution of MSE with respect to the number of reconstruction iterations for the three considered algorithms.

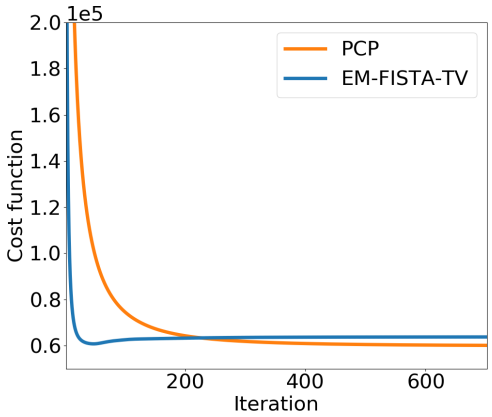

Fig. 4: Evolution of the cost function $d_{KL}(Af^{(n)}, p) + \beta TV(f^{(n)})$ with the the number of iterations. Due to the FISTA acceleration, EM-FISTA-TV is not always decreasing.

In terms of number of projections and back-projections (Fig. 3), EM-FISTA-TV is much faster than the two others. However, one iteration has different costs for the three algorithms. Figure 5 shows the MSE as a function of the computation time for the two fastest algorithms, PCP and EM-FISTA-TV. The reconstruction results we obtain are similar for the two inversion approaches although the second is faster to converge.

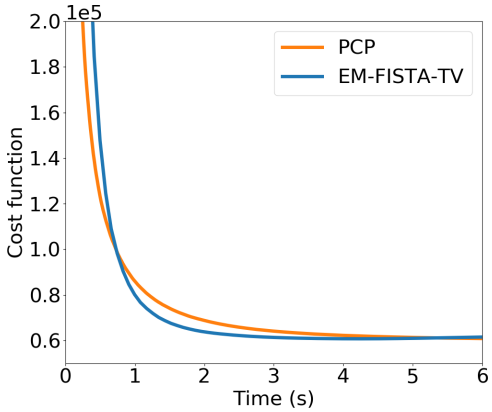

Fig. 5: Convergence as function of the total execution time, on a Quadro P2000 GPU card.

C. Application to experimental data tests

We show here a preliminary result obtained with the EM-FISTA-TV algorithm for a three-dimensional sample of CoOCNT observed in transmission electron microscopy.

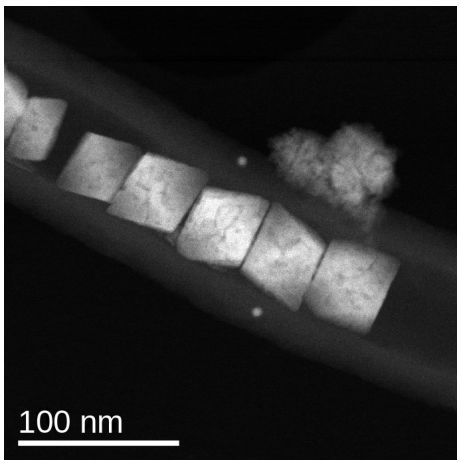

Fig. 6: Slice of the noisy projections of CoOCNTs sample

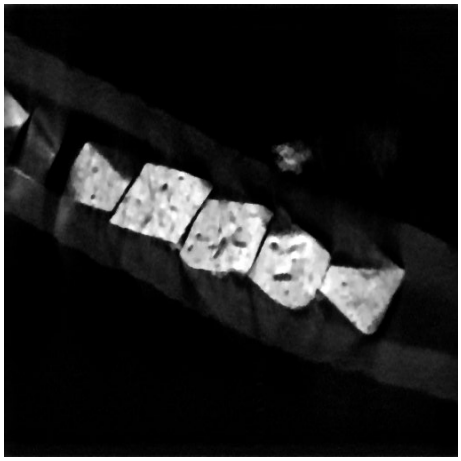

Fig. 7: Slice of the reconstructed image of CoOCNTs with EM-FISTA-TV algorithm

The mixed Poisson-Gaussian noise model is adapted to this imaging modality [19]. Faceted cobalt–cobalt oxide based nanoparticles (NPs) with high density and narrow size distribution (50 ± 5 nm) were selectively cast inside the channels of multi-walled carbon nanotubes (CNTs) through the controlled thermal decomposition of cobalt stearate in the presence of oleic acid as surfactant. A number of 59 projections of the sample, ranging from -70 to 75 degrees were acquired. One example of projection is shown in Fig. 6. We reconstructed a 3D-volume with dimensions 512^3 pixels with regularization parameter $\beta = 0.8$. Figure 7 shows a slice of the reconstructed volume. We cannot compute MSE for real data, but results for SIRT-FISTA-TV and PCP are visually very similar. Moreover, we can see in Figure 8 that convergence was faster for EM-FISTA-TV in our experiments, considering the cost function decay.

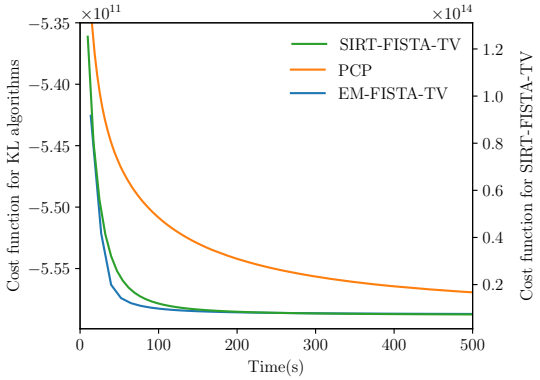

Fig. 8: Cost function decay with respect to the algorithm running time for reconstructions on real TEM data. The cost function of PCP and EM-FISTA-TV is different than the one for SIRT-FISTA-TV, thus the latter has been represented on a different scale. However the speed of convergence can be captured in this graph. Here computation was performed on a NVIDIA Tesla V100 GPU.

IV. Discussions

Our results tend to indicate that for a similar contribution of Poisson and Gaussian components in the overall noise, the quality of reconstruction is slightly inferior for SIRT-FISTA-TV compared to the PCP and EM-FISTA-TV algorithms. EM-FISTA-TV requires less iteration than the PCP to reach the solution. Nevertheless, one needs to remember the structure of these two algorithms. Indeed, the first one has an internal loop that aims at denoising the MLEM-reconstructed image at each iteration. For the second one, the whole reconstruction process, TV denoising included, is performed in a single loop. In that sense, it is interesting to check convergence as a function of total computation time. In our tests, EM-FISTA-TV is the fastest approach. However, these results are strongly dependent on several factors and may change from one application to another. First, the number of iterations in the denoising part is chosen to insure convergence in the internal loop, though there is no indication that less iterations inside this loop could lead to a similar final solution - and thus in a smaller computation time. Second, the results depend on the implementation and will not be the same if, for instance, CPU would be used instead of GPU for denoising. Finally, the result depends on the ratio between the cost of one projection/back-projection pair and the cost of the denoising algorithm. To conclude, EM-FISTA-TV and PCP gave more accurate reconstructions as for the MSE, but results on convergence largely depend on implementation details. However on TEM data, EM-FISTA-TV was the fastest algorithm to converge.

This study was performed with a particular setting of noise. We saw that when applied to TEM data, results on convergence were similar to our experiments, but a deeper study would be necessary in order to assess these trends on a larger set of noise configurations. However, the choice of the regularization parameter for each of these configurations would probably be a challenge to address.

V. Conclusion

In this work, we have compared several iterative algorithms based on TV regularization for tomographic reconstruction with a mixture of Poisson and Gaussian noise. They are tested on both simulated and real data. The EM-FISTA-TV gave the best reconstruction results in terms of computation time and reconstruction accuracy.

References

[1] R. Gordon, R. Bender, and G. T Herman. Algebraic reconstruction techniques (ART) for three-dimensional electron microscopy and X-ray photography. *Journal of theoretical Biology*, 29(3), 1970.

[2] A. H Andersen and A. C Kak. Simultaneous algebraic reconstruction technique (SART): a superior implementation of the ART algorithm. *Ultrasonic imaging*, 6(1), 1984.

[3] P. Gilbert. Iterative methods for the three-dimensional reconstruction of an object from projections. *Journal of theoretical biology*, 36(1), 1972.

[4] K. Lange and R. Carson. EM reconstruction algorithms for emission and transmission tomography. *J Comput Assist Tomogr*, 8(2), 1984.

[5] A.P. Dempster, N.M. Laird, and D.B. Rubin. Maximum likelihood from incomplete data via the EM algorithm. *Journal of the Royal Statistical Society: Series B (Methodological)*, 1977.

[6] H. Banjak, T. Grenier, T. Epicier, S. Koneti, L. Roiban, A.-S. Gay, I. Magnin, F. Peyrin, and V. Maxim. Evaluation of noise and blur effects with SIRT-FISTA-TV reconstruction algorithm: Application to fast environmental transmission electron tomography. *Ultramicroscopy*, 189:109–123, 04 2018.

[7] A. Sawatzky, C. Brune, F. Wübbeling, T. Kösters, K. Schäfers, and M. Burger. Accurate EM-TV algorithm in PET with low SNR. In *Nuclear Science Symposium*, 2018.

[8] V. Maxim, Y. Feng, H. Banjak, and E. Bretin. Tomographic reconstruction from Poisson distributed data: a fast and convergent EM-TV dual approach. preprint, INSA Lyon, https://hal.archives-ouvertes.fr/hal-01892281/, 2018.

[9] F. Benvenuto, A. La Camera, C. Theys, A. Ferrari, H. Lanteri, and M. Bertero. The study of an iterative method for the reconstruction of images corrupted by Poisson and Gaussian noise. *Inverse Problems*, 24(3):1085–1088, 2008.

[10] A. Jezierska, E. Chouzenoux, J.-C. Pesquet, and H. Talbot. A primal-dual proximal splitting approach for restoring data corrupted with Poisson-Gaussian noise. In *2012 IEEE International Conference on Acoustics, Speech and Signal Processing (ICASSP)*, 2012.

[11] F. Murtagh, J.L. Starck, and A. Bijaoui. Image restoration with noise suppression using a multiresolution support. *Astronomy and Astrophysics supplement*, 112, 1995.

[12] A. Chambolle and T. Pock. A first-order primal-dual algorithm for convex problems with applications to imaging. *JMIV*, 40(1), 2011.

[13] L. I Rudin, S. Osher, and E. Fatemi. Nonlinear total variation based noise removal algorithms. *Physica D: nonlinear phenomena*, 60(1-4), 1992.

[14] E. Y Sidky, C.-M. Kao, and X. Pan. Accurate image reconstruction from few-views and limited-angle data in divergent-beam CT. *Journal of X-ray Science and Technology*, 14(2), 2006.

[15] T. Pock and A. Chambolle. Diagonal preconditioning for first order primal-dual algorithms in convex optimization. In *Proceedings / IEEE International Conference on Computer Vision*, 2011.

[16] A. Chambolle. An algorithm for Total Variation Minimization and Applications. *Journal of Mathematical Imaging and Vision*, 20, 2004.

[17] A. Beck and M. Teboulle. A fast iterative shrinkage-thresholding algorithm for linear inverse problems. *SIAM Journal on Imaging Sciences*, 2(1), 2009.

[18] W. van Aarle, W. J Palenstijn, J. De Beenhouwer, T. Altantzis, S. Bals, K. Joost Batenburg, and J. Sijbers. The ASTRA Toolbox: A platform for advanced algorithm development in electron tomography. *Ultramicroscopy*, 157, 2015.

[19] O. Öktem. Reconstruction methods in electron tomography. 2008.